Hindawi
Shock and Vibration
Volume 2023, Article ID 3334033, 8 pages
https://doi.org/10.1155/2023/3334033

Research Article

Experimental Study of Penetration Capability of an Annular-Shaped Charge under Multipoint Synchronous Initiation

Liu Jie,[1] **Hong Qing**,[1] **Gao Jiandong**,[2] **Chen Xi**,[2] **and Du Zhonghua**[2]

[1]*School of Mechanical Engineering, Nanjing Vocational University of Industry Technology, Nanjing 210023, China*
[2]*School of Mechanical Engineering, Nanjing University of Science and Technology, Nanjing 210094, China*

Correspondence should be addressed to Liu Jie; 2019101054@niit.edu.cn

Received 15 March 2023; Revised 25 April 2023; Accepted 18 May 2023; Published 29 May 2023

Academic Editor: FuRen Ming

The large-distance penetration capability of an annular-shaped charge under multipoint synchronous initiation was experimentally investigated. For different annular charge structures and different multipoint initiation settings, incident angle, collision type of detonation waves, and overpressure on the shaped charge's liner at adjacent initiation points were analyzed using the detonation wave propagation theory. Furthermore, the shaped charge's penetration capability at a standoff distance of 1–15 m from a 20 mm thick 45# steel plate (the target) was determined through penetration experiments. It was found that the annular cutter formed by the 500 mm diameter annular shaped charge (charge width: 100 mm) completely penetrated the target for a large distance, namely a distance of 150 times the charge width. The ratio of the width of the ring gap penetrated by the annular cutter to the liner's initial radial width was about 1.07; this indicated that the annular cutter's width was equivalent to the liner's radial width for the above flight distance, which in turn implied that the annular cutter had superior circular degree. The annular cutter formed in the case of Mach reflection had better circular degree, integrity, and penetration capability than that formed by regular reflection.

1. Introduction

An annular-shaped charge is a typical example in engineering applications of explosion mechanics which is achieved through the controllable formation of the liner. Compared with a single jet or projectile, it can penetrate a larger area and cause more damage to a target at a long distance [1]. Currently, the typical cross-section of the liner commonly used on an annular-shaped charge is V-shaped. After detonation, the instantaneous detonation pressure causes the V-shaped liner to form a high-speed jet cutter [2]. An annular-shaped charge is widely used for rock cutting, underwater cutting, and concrete cutting, apart from being used in many processes [3]. When its underside comes in contact with a target or is at a standoff distance of five times the charge width from the target, the penetration capability of the target by the charge after initiation is apparent [2, 3]. However, when the standoff distance from the target is increased to 10 times the charge width, the annular cutter formed by the liner breaks before reaching the target, resulting in a reduced penetration depth. The main reasons for the breaking are improper initiation and inappropriate design of the structures of the charge and liner. There have been few studies on the penetration capability of an annular cutter at a large distance, and studies on the forming process and integrity of an annular-shaped charge are also sparse. Experimental studies on the penetration capability of an annular-shaped charge at a large distance are rare since they are difficult and challenging to perform, which is mainly manifested in the following two points. According to the current research, the maximum flight distance of an annular cutter is about 50 times the diameter or width of the charge [4]. Beyond this distance, the annular cutter easily breaks into several pieces and no longer maintains the original annular shape. In other words, beyond this distance, its penetration capability is reduced. Second, the circular radius of the cutter gradually increases with an increase in the flight distance. After reaching the target, the annular cutter's

radius is larger than its initial radius, resulting in a larger circumferential velocity gradient on the annular cutter and a smaller cross-sectional area of the annular cutter. Consequently, the effective mass of the cutter's section is reduced, which reduces the cutter's penetration capability. It is known that the performance of the annular cutter in engineering applications worsens at a larger standoff distance from the target. In summary, if the annular-shaped charge is to have high penetration capability at a large distance, it should have a satisfactory and consistent circumferential velocity, an appropriate circular degree, and a sufficiently symmetric radial structure. To examine ways to overcome the drawbacks of the annular cutter, this study chose an annular-shaped charge with a diameter (d) of 500 mm (with an inner diameter of 400 mm and a charge width of 100 mm) and a height (h) of 50 mm as the research object. The shaped charge is shown in Figure 1.

In this study, by setting multipoint synchronous initiation and using the detonation wave propagation theory, we obtained the overpressure on the surface of the liner for two types of reflections of detonation waves that have undergone collision in the shaped charge, namely regular reflection and Mach reflection. Furthermore, the penetration capability of the annular cutter was examined by performing experiments that involved standoff distances of 10–150 times the charge width. This study successfully improved the penetration capability of the annular shaped charge and provides significant experimental support for engineering applications of the annular-shaped charge involving large standoff distances.

2. Interaction Analysis of Detonation Waves in Annular-Shaped Charge

2.1. Analysis of Interaction of Detonation Waves. In Figure 2, the *xoy* plane is the symmetry plane at the centerline between the inside and outside diameters of the unit charge. The initiation points are distributed along the x-axis, and the circle on which the initiation points are distributed is the aforementioned centerline. The circumference (L) of the circle is given by $L = d\pi$. The arc length between adjacent initiation points corresponds to a central angle (α) of 10°. The distance between adjacent initiation points is determined from the following chord length equation:

$$c = d\sin\left(\frac{\alpha}{2}\right). \tag{1}$$

The coordinates of the two initiation points are $((d/2)\sin(\alpha/2), 0, 0)$ and $(-(d/2)\sin(\alpha/2), 0, 0)$, and the height of the charge is denoted by h. The distance between the two initiation points is the chord length c. In the *xoy* plane, when the two initiation points are detonated simultaneously, the hemispherical detonation waves generated propagate independently at the same speed. With an increase in the incident angle, the two detonation waves collide and undergo regular reflection and Mach reflection in sequence.

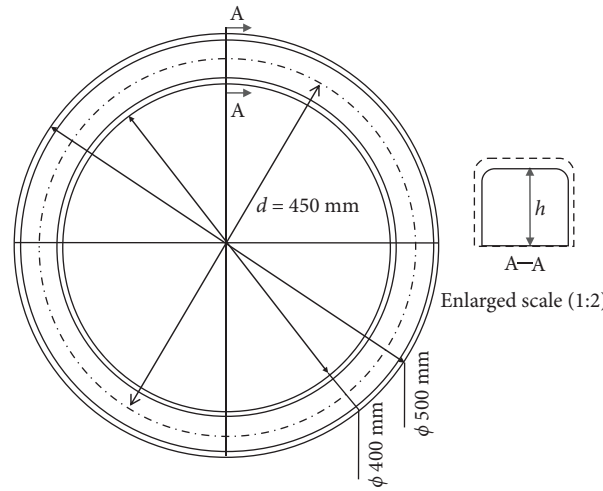

Figure 1: Diagram of the 500 mm diameter annular-shaped charge.

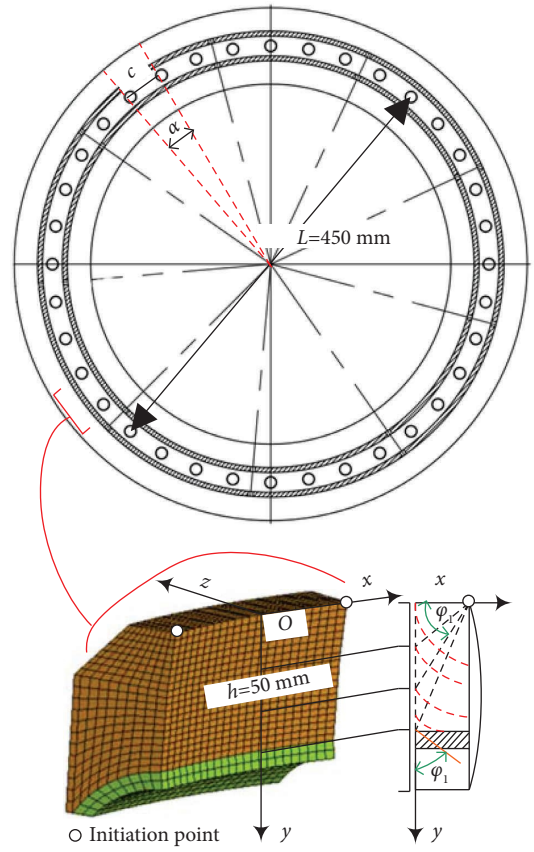

Figure 2: Schematic of detonation wave propagation in the unit charge.

The two detonation waves come into contact at the coordinate origin O_c and undergo normal collision. Subsequently, the collision point moves in the positive y-axis direction, and the normal collision changes into a regular reflection. The incident angle φ_1 formed between the tangent line of the wave front and the y-axis in Figure 2 is calculated.

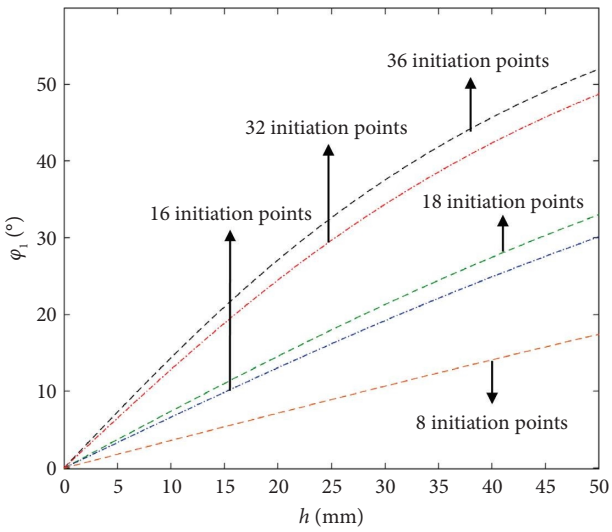

Figure 3: Plots of the incident angle against the charge height.

From the geometric relation, the following expression can be obtained:

$$\varphi_1 = \arctan\frac{2y}{c};\ [0 \le y \le h]. \tag{2}$$

This equation describes the change in the incident angle in the *xoy* plane with the charge height, and curves obtained using this equation are shown in Figure 3. Figure 3 contains different numbers of initiation points. For example, the incident angle ranges corresponding to 36 and 18 initiation points are 0°–52° and 0°–33°, respectively, and they are independent of each other.

A schematic of the collision process of detonation waves in the unit charge is shown in Figure 4. The wave system includes the common conventional regular reflection and Mach reflection, and it comprises the incident wave *I*, reflected wave *R*, and Mach stem [5–8]. The actual collision point O_c lies on the axis of symmetry and moves in the positive *y*-axis direction, and the detonation velocity of the CJ wave front is denoted by D_{CJ}. O_c of the wave system is fixed, and the flow field is divided into three regions. The incident angle of the detonation wave is denoted by φ_1, the deflection angles of incoming flow passing through the incident wave and reflected wave are denoted by θ_1 and θ_2, respectively, and the angle (reflection angle) between the reflected wave and the wall surface is denoted by φ_2. The deflection angle of the incoming flow after passing through the Mach stem is θ_1-θ_2 [9–13]. According to the Rayleigh–Hugoniot relationship, the incident angle φ_1 and deflection angle θ_1 from regions (0) to (1) have the following relationship:

$$\tan\theta_1 = \frac{\tan\varphi_1}{\gamma\tan^2\varphi_1 + \gamma + 1}, \tag{3}$$

where γ is the polytropic exponent that can be calculated from the following formula:

$$\gamma = \frac{\rho_0 D_{CJ}^2}{P_{CJ}} - 1, \tag{4}$$

here, ρ_0 and P_{CJ} are the initial density of explosives and the CJ pressure, respectively.

In the wave system, the incoming flow first passes through the incident wave and then the reflected wave, and it then becomes parallel to the collision line. Hence, the two deflections are equal, as shown in the following equation:

$$\theta_1 = \theta_2. \tag{5}$$

According to the Rayleigh–Hugoniot relationship, for regular reflection, the incident angle φ_1 and deflection angle θ_1 in the wave system have the following relationship:

$$\tan\varphi_2 = \frac{(\gamma-1)\left[M_1\sin(\varphi_2+\theta_1)\right]^2 + 2}{(\gamma+1)\left[M_1\sin(\varphi_2+\theta_1)\right]^2}\tan(\varphi_2+\theta_1). \tag{6}$$

Similarly, for Mach reflection, φ_1 and θ_1 in the wave system have the following relationship in the flow field from regions (0) to (3):

$$\tan\varphi_2 = \frac{(\gamma-1)\left[M_1\sin(\varphi_2+\theta_1-\theta_2)\right]^2 + 2}{(\gamma+1)\left[M_1\sin(\varphi_2+\theta_1-\theta_2)\right]^2}\tan(\varphi_2+\theta_1-\theta_2), \tag{7}$$

where M_1 is the Mach number of zone (1) and is given by

$$M_1 = \sqrt{1+\left(\frac{1+\gamma}{\gamma\tan\varphi_1}\right)^2}. \tag{8}$$

The charge is *B* explosive, with a density (ρ_0) of 1.65 g/cm^3. The polytropic exponent is 1.69, the detonation velocity is 7452 m/s, and the critical angle (φ_c) for transition from regular reflection to Mach reflection is 50.71°, which is comparable to the incident angle range in Figure 3.

According to the works of Sternberg et al. [13–16], the ratio between the pressure in regions (1) and (2) is given by

$$\frac{P_2}{P_{CJ}} = \frac{2\gamma\left[M_1\sin(\varphi_2+\theta_1)\right]^2}{1+\gamma} - \frac{\gamma-1}{\gamma+1}. \tag{9}$$

The following equation can be used to calculate the detonation pressure of the Mach stem corresponding to φ_1:

$$\frac{P_3}{P_{CJ}} = \left(\frac{\sin\beta}{\sin\varphi_1}\right)^2 + \frac{\sin\beta}{\sin\varphi_1}\sqrt{0.8\left(\frac{\sin\beta}{\sin\varphi_1}\right)^2 - 0.8}, \tag{10}$$

here, β is the angle between the Mach stem and the collision line. In this study, the Mach stem was assumed to be perpendicular to the collision line, and hence, β was 90°. The CJ detonation pressure P_{CJ} can be calculated from equation (4). The pressure intensity in the Mach reflection region and regular reflection region was calculated from equations (9) and (10), and it is shown in Figure 5.

In Figure 5, the incident angle range for 36 initiation points is in the Mach reflection region, while that for 18 initiation points is in the regular reflection region. The calculation results in the figure show that the overpressure ratio for Mach reflection is about 15% higher than that for regular reflection, which indicates a high circular degree,

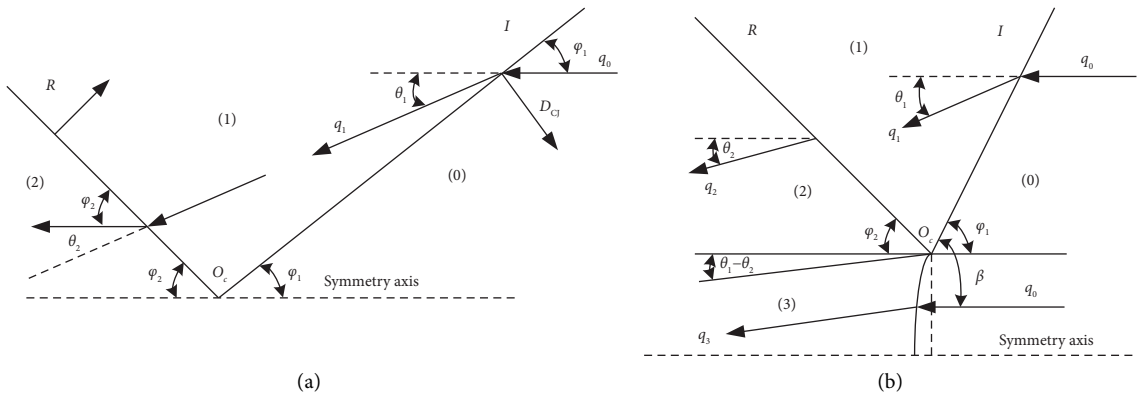

Figure 4: Typical types of detonation wave collisions. (a) Regular reflection. (b) Mach reflection.

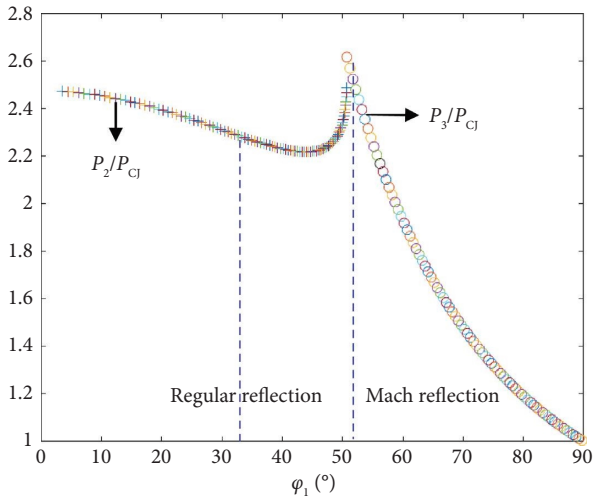

Figure 5: Pressure intensity in the regular reflection and Mach reflection regions.

high integrity, and high penetration capability of the annular cutter. Penetration experiments (described in the next section) were conducted to ascertain the difference between regular reflection and Mach reflection and the penetration capability of the annular cutter.

3. Experiments on the Penetration Capability of an Annular-Shaped Charge

3.1. Description of the Schematic Diagram of the Penetration Experiment. Using a synchronous disk-shaped multipoint initiation device, we performed penetration experiments to determine the penetration capability of an annular-shaped charge. The formation, circular degree, and penetration capability of the shaped charge were analyzed in depth in a static experiment. B explosive was used in the annular-shaped charge, and the material of the liner was T2 copper. The shell of the explosive was made of aluminum alloy and was 2 mm thick. A 45# steel plate with a thickness of 20 mm and dimensions of 1.5 m × 1.5 m was chosen as the target. Both the target and annular shaped charge were supported by wooden frames, and the horizontal distance L_f between them was set to be 1, 5, 10, and 15 m. Eight sets of experiments were sequentially performed: four sets with 36-point synchronous initiation, one set with 8-point synchronous initiation, one set with 16-point synchronous initiation, and two sets with 32-point synchronous initiation. A thin aluminum foil device was positioned between the target and shaped charge for speed measurement, and a synchronous device was used to maintain the initiation synchronicity error below 1 μs to minimize the effect of initiation deviation [16, 17]. A schematic of the setup of the above experiments is shown in Figure 6.

3.2. Analysis of Penetration Experiment Results. The results of the penetration experiments, shown in Table 1, were compared and analyzed. At horizontal distances of 1, 5, and 10 m, the average diameters of the perforated holes were 450, 455, and 453 mm, respectively. The annular cutter completely penetrated the 45# steel target, and the inner surfaces of the circular perforated holes were smooth. The holes formed by the penetration had a high circular degree, which indicated that the cutter could maintain its annular shape over a large distance without breaking. This also showed that the annular cutter had an effective penetration at a standoff distance of 100 times the charge width. The average velocity V_f of the annular cutter was measured to be about 1600 m/s. At a horizontal distance of 15 m, the cutter could penetrate the 45# steel target, and the outline of the hole on the target after penetration was L-shaped, indicating the fracture and rotation of the annular cutter during flight. For the distance of 15 m, an annular cutter could also penetrate the 45# steel target, and the resulting perforation was L-shaped, indicating the fracture and rotation of the circular cutter during the flight process. The scattered materials of the cutter were partially dispersed, and some of them were embedded close to the center of the inner circle, leading to columnar formation after the explosion.

The results of the penetration experiments, shown in Figure 7, were compared under different numbers of initiation points at horizontal distances of 10 m. For the conditions of 8 initiation points and 16 initiation points, no obvious holes were formed on the target under penetration of the annular cutter. Therefore, the penetration effect in

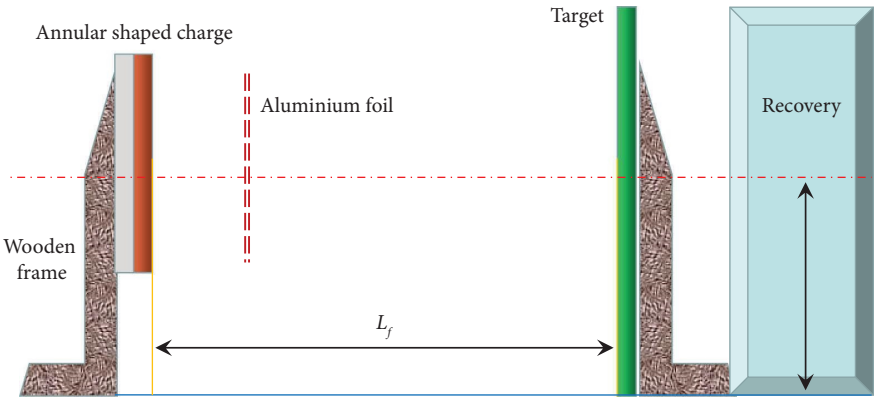

Figure 6: Schematic of the setup of the penetration experiments involving an annular-shaped charge.

Table 1: Results of a penetration experiment involving an annular shaped charge at different standoff distances (36 initiation points).

Sites				
Traces				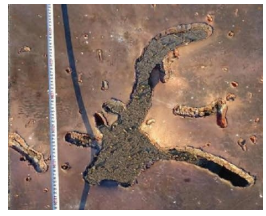
ϕ_c	450 mm	455 mm	453 mm	190 mm "L": 245 mm × 205 mm
V_f		1604.9 m/s	1600 m/s	
L_f	1 m	5 m	10 m	15 m

these two sets of experiments was less effective. The annular-shaped charge with 32 detonation points penetrated the target plate and formed a hole. The average diameter of the perforated holes was 410 mm. Although the inner edges of the circular perforated holes were irregular, it also indicated that the more detonation points there are, the better the integrity of the annular cutter and the better the penetration effect.

A quarter of the annular-shaped charge was chosen, and four equidistant initiation points were set on this part. A penetration experiment with these initiation points was conducted with uneven synchronous initiation, as shown in Figure 8. A distribution of detonation points on the quarter of the charge was equivalent to 18 initiation points uniformly distributed on the charge. In Figure 9, it is apparent that after the 32 initiation points of the annular shaped charge detonated synchronously, the detonation waves generated by one quarter of the annular shaped charge and the other three quarters collided with each other. On the basis of the variation range of the calculated incident angles in Figure 3, the type of collision in the case of the detonation waves generated by one quarter of the annular-shaped charge was regular reflection, and the type of collision in the case of detonation waves generated by the other three quarters was Mach reflection. Both types of collisions and reflections occurred on the surface of the liner. Therefore, the type of detonation wave collision in the charge was determined by the distribution of the initiation points, and the type of detonation wave collision indirectly affected the formation of the annular cutter. A ring gap was observed in the experiment involving uneven synchronous initiation points, and the average width w_p of the ring gap after the annular cutter penetrated the target from a distance of 10 m was about 60.07 mm. Since the initial width w_r of the liner in the charge was 56.1 mm, the width ratio between the two was about 1.07. From this ratio, it was inferred that the width of the ring gap was roughly equal to the initial width of the liner at a standoff distance of 100 times the charge width. Apart from two small holes in the penetration area of the target corresponding to one quarter of the annular-shaped charge,

(a) (b) (c)

Figure 7: Different numbers of initiation points (L_f: 10 m). (a) 8 initiation points. (b) 16 initiation points. (c) 32 initiation points.

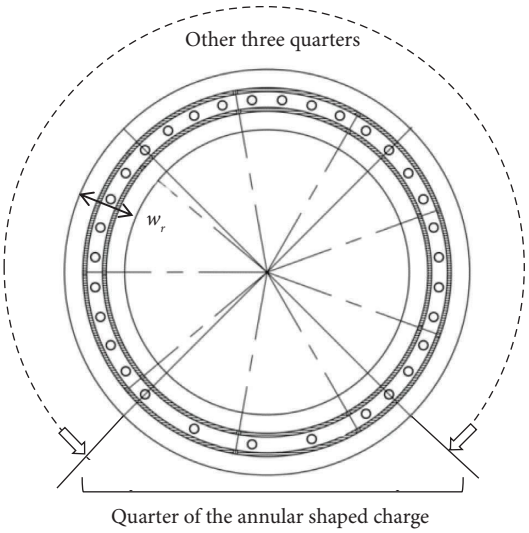

Figure 8: Schematic of uneven synchronous initiation points.

Figure 9: Ring gap extending along the uneven synchronous initiation points.

there were long strips of penetration traces that were not penetrated. By contrast, the penetration area corresponding to the other three quarters of the charge was completely penetrated. It was also evident that the effect of the Mach reflection of the detonation wave was better than that of the regular reflection.

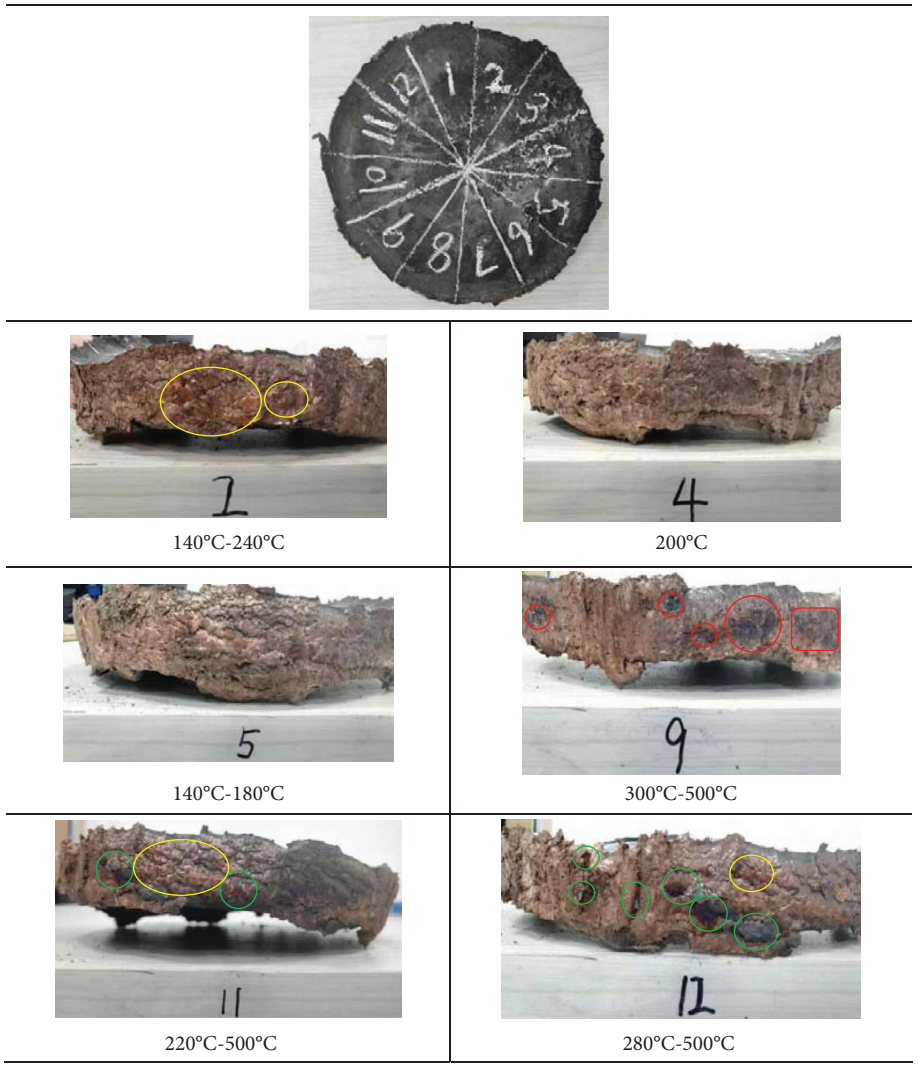

Figure 10: Circumferential cross-section of the target and the distribution of the residual oxide.

4. Analysis of the Circumferential Cross-Section of the Target

Figure 10 shows experimental observations after the penetration of the target by the annular cutter. The oxide color on the circumferential section of the target showed that the temperature rise of the liner material and the target was considerably lower than the melting points of T2 pure copper and 45# steel. The surface of the penetrated target was divided into twelve equal parts and labeled with numbers from 1 to 12.

These twelve parts showed the morphology of the circumferential section of the target and the distribution of the remaining copper oxide. The residual copper oxidation products were CuO (the main product) and small amounts of pure copper and Cu_2O [18]. The color of the residual oxide in region 2 was brass-colored or gold-colored, indicating that the temperature range of the residual oxide during the oxidation reaction was between 140°C and 240°C. The color of the residual oxide in regions 4 and 5 was mainly dark yellow; thus, the temperature range of the residual oxide during the oxidation reaction was mainly between 140°C and 200°C. The color distribution of the residual oxide in region 9 was uneven, and there were brown and black spots. This indicated that the temperature range of the residual oxide during the oxidation reaction was about 300°C to 500°C. The color of the residue in regions 11 and 12 was mainly black and magenta, indicating a temperature range of 220°C to 500°C for the residue during the oxidation reaction. Thus, it was verified that the annular cutter formed at the instant of the charge explosion was not molten copper [19] and that the liner transformed into a fluid after being subjected to extremely high pressure.

5. Conclusion

For multipoint synchronous initiation and appropriate design of the structures of the charge and liner, the large penetration capability of the annular cutter in the case of Mach reflection occurring during the detonation wave collision was more effective and apparent than that in the case of regular reflection as the former enhanced the

integrity and circular degree of the cutter in the circumferential direction. The average width of the ring gap formed by the annular cutter as it penetrated the target was roughly equal to the initial width of the liner in the case of Mach reflection, which indicated that the distribution of the initiation points indirectly affected the formation of the annular cutter. The temperature range of the residual oxide on the circular section of the penetrated target during the oxidation process was between one-third and one-half of the temperature of copper's melting point and was unevenly distributed.

Data Availability

The data used to support the findings of this study are included within the article.

Conflicts of Interest

The authors declare that they have no conflicts of interest.

Acknowledgments

The work presented in this paper has been supported by the Open Fund Project (ZK21-05-14) of Jiangsu Industrial Sensing and Intelligent Manufacturing Equipment Engineering Research Center.

References

[1] W. Wang, Z. Chen, B. Yang, T. Jing, F. Meng, and T. Zhao, "Formation of an explosively formed penetrator warhead using a step-shaped charge," *Shock and Vibration*, vol. 2022, Article ID 9694576, 17 pages, 2022.

[2] K. L. Phelps, *Material Properties Affecting the Penetration of Metal Targets by Copper Linear Shaped Charges*, Missouri University of Science and Technology, Rolla, MO, USA, 2016.

[3] B. T. Burch, *Determining and Mitigating the Effects of Firing a Linear Shaped Charge under water*, Missouri University of Science and Technology, Rolla, MO, USA, 2014.

[4] M. Huerta and M. G. Vigil, "Design, analyses, and field test of a 0.7m conical shaped charge," *International Journal of Impact Engineering*, vol. 32, no. 8, pp. 1201–1213, 2006.

[5] J. Liu, X. Chen, and Z. Du, "A study on the surface overpressure distribution and formation of a double curvature liner under a two-point initiation," *Defence Technology*, vol. 18, no. 1, pp. 148–157, 2022.

[6] K. N. Panov, V. A. Komrachkov, and I. S. Tselikov, "Radiographic study of interaction of shock and detonation waves in a high explosive," *Combustion, Explosion and Shock Waves*, vol. 43, no. 3, pp. 365–371, 2007.

[7] Y. Wang, W. Li, J. Yu, W. Li, and H. Xu, "Research on numerical simulation of tantalum explosively formed projectile forming driven by detonation," *Shock and Vibration*, vol. 2022, Article ID 2175801, 13 pages, 2022.

[8] Y. Liu, J. Yin, and Z. Wang, "Study on the overdriven detonation wave propagation in double-layer shaped charge," *Physics of Fluids*, vol. 31, p. 9, 2019.

[9] B. B. Dunne, "Mach reflection of detonation waves in condensed high explosives," *Physics of Fluids*, vol. 4, no. 7, pp. 918–933, 1961.

[10] B. B. Dunne, "Mach reflection of detonation waves in condensed high explosives II," *Physics of Fluids*, vol. 7, no. 10, pp. 1707–1712, 1964.

[11] L. M. Hull, *Detonation Propagation and Mach Stem Formation in PBXN-9*, Los Alamos National Lab, Los Alamos, NM, USA, 1997.

[12] L. M. Hull, *Mach Reflection of Spherical Detonation Waves*, Nuclear Regulatory Commission, Washington, DC, USA, 1993.

[13] H. M. Sternberg and D. Piacesi, "Interaction of oblique detonation waves with iron," *Physics of Fluids*, vol. 9, no. 7, pp. 1307–1315, 1966.

[14] J. Pan, X. Zhang, Y. He, Q. Deng, and Z. Guan, "Theoretical and experimental study on detonation wave propagation in cylindrical high explosive charges with a wave-shaper," *Central European Journal of Energetic Materials*, vol. 13, no. 3, pp. 658–676, 2016.

[15] C. S. Zhu, Z. X. Huang, X. D. Zu, and Q. Q. Xiao, "Mach wave control in explosively formed projectile warhead," *Propellants, Explosives, Pyrotechnics*, vol. 39, no. 6, pp. 909–915, 2014.

[16] R. Li, W. B. Li, X. M. Wang, and W. B. Li, "Effects of control parameters of three-point initiation on the formation of an explosively formed projectile with fins," *Shock Waves*, vol. 28, no. 2, pp. 191–204, 2017.

[17] R. Li, W. Li, X. Guo et al., "Groove charge of a rigid multipoint initiation explosive network," *Propellants, Explosives, Pyrotechnics*, vol. 43, no. 9, pp. 929–938, 2018.

[18] M. Walkowicz, P. Osuch, B. Smyrak et al., "Impact of oxidation of copper and its alloys in laboratory-simulated conditions on their antimicrobial efficiency," *Corrosion Science*, vol. 140, pp. 321–332, 2018.

[19] A. Doig, "Some Metallurgical Aspects of Shaped Charge Liners," *Journal of Battlefield Technology*, vol. 1, no. 1, 1998.